Resonant transfer and excitation in collisions of chlorinelike ions with H_2 targets

Mau Hsiung Chen
High Temperature Physics Division, Lawrence Livermore National Laboratory, Livermore, California 94550
(Received 18 September 1991)

The resonant transfer and excitation cross sections through the *LMM* transitions in collisions of chlorinelike Fe^{9+}, Nb^{24+}, and La^{40+} with H_2 targets were calculated in impulse approximation using the multiconfiguration Dirac-Fock method. The effect of relativity reduces the total *LMM* resonance strength for La^{40+} by 29%. The angular distribution corrections at $\theta=90°$ increase the cross sections by an amount less than 10%. The present theoretical predictions for La^{40+} colliding with H_2 are in reasonable agreement with the experimental observations.

PACS number(s): 34.70.+e, 34.80.Kw

I. INTRODUCTION

Resonant transfer and excitation in collisions of multiply charged ions with atoms or molecules is a correlated two-electron process. It can occur when the projectile energy is in resonance to excite the ion and capture a target electron simultaneously in a single collision to form a doubly excited state. This autoionizing state formed by the resonant transfer and excitation can decay by x-ray emission (RTEX) or Auger transition (RTEA) [1,2]. RTEX is an atomic process analogous to dielectric recombination (DR). The only difference between them is the capture of a free electron instead of a weakly bound target electron in a DR process. There are other nonresonant transfer excitation processes in ion-atom collisions. The same resonance states as in RTEX can be formed by collisions with target nucleus (NTE) [3]. The projectile can also be excited by collisions with a target electron, and the other target electron can be transferred to the projectile (2 *e* TE) [3]. Here, we are only concerned with the resonant RTEX process.

There have been many experimental [2,4–8] and theoretical studies [1,3,9–14] on the RTEX process in ion-atom collisions. These investigations are mainly concentrated on collision systems involving Li-like ions with atomic number $Z<36$ and K-shell excitation. Recently, ions as heavy as U^{89+} and U^{90+} have been studied both experimentally [8] and theoretically [13,15]. The importance of the relativistic effect on DR or RTEX cross sections has clearly been demonstrated. Currently, few data exist for the RTEX process in a complex ion involving L-shell excitation. The lone experimental work [16] on projectile charge-state dependence for L-shell excitation yields results in disagreement with theoretical predictions [14,16]. In this paper we report on the calculations of L-shell RTEX via *LMM* transitions in collisions of chlorinelike ions (i.e., Fe^{9+}, Nb^{24+}, and La^{40+}) with H_2 targets in an impulse approximation [1]. The required atomic data such as energies, radiative, and Auger transition rates were calculated from perturbation theory using the multiconfiguration Dirac-Fock (MCDF) method [17,18]. The theoretical results for La^{40+} are compared with the only experimental data [19] for this isoelectronic sequence. The effect of relativity on L-shell RTEX cross sections is also examined.

II. CALCULATIONAL PROCEDURE

In the present work, we employ the impulse approximation pioneered by Brandt [1] for calculating the RTEX cross sections with modifications including the target electron binding energy [20] and the effect of angular distribution [21]. In this approximation, it is assumed that the collision velocity is much larger than the orbital velocity of the target electrons and the distortion of the projectile resonance state by the target nuclear is very small. The total RTEX cross section $\sigma^x_{\mathrm{RTE}}(i)$ for an initial state i can then be obtained from the DR cross section $\bar{\sigma}_{\mathrm{DR}}$ by folding with the Compton profile $J(Q)$ of the target atoms or molecules,

$$\sigma^x_{\mathrm{RTE}}(i)=\sum_{d,f}(M/2E)^{1/2}\Delta E\,\bar{\sigma}_{\mathrm{DR}}(i\,df)J(Q)W(\theta)\ , \tag{1}$$

where

$$Q=(E_d+E_t-Em/M)(M/2E)^{1/2}\ . \tag{2}$$

Here, E is the projectile energy in the laboratory frame; M and m are the masses of the projectile and electron, respectively; ΔE and E_d are the energy bin width and the Auger energy for the intermediate state d, respectively; and E_t is the target electron binding energy.

The energy-averaged DR cross section is calculated in an isolated resonance approximation:

$$\bar{\sigma}_{\mathrm{DR}}(i\,df)=\frac{\pi^2}{\Delta E E_d}\frac{g_d}{2g_i}\frac{A_a(d\rightarrow i)A_r(d\rightarrow f)}{\sum_j A_a(d\rightarrow i)+\sum_k A_r(d\rightarrow k)}\ , \tag{3}$$

where g_d and g_i are statistical weight factors for the states d and i, respectively; $A_a(d\rightarrow i)$ is the Auger rate and $A_r(d\rightarrow k)$ is the radiative rate; and atomic units are used in Eq. (3).

The angular distribution function $W(\theta)$ averaged over

the polarization for the electric dipole transition is given by

$$W(\theta)=1+\beta_2 P_2(\cos\theta) , \tag{4}$$

with the anisotropic parameter

$$\beta_2=(-1)^{1+J_i+J_f}\left[\frac{3(2J_i+1)}{2}\right]^{1/2}\begin{Bmatrix}1 & 1 & 2\\ J_i & J_i & J_f\end{Bmatrix}\frac{P^{(2)}_{J_0J_i}}{P^{(0)}_{J_0J_i}} , \tag{5}$$

and

$$P^{(L)}_{J_0J_i}=\frac{1}{2(2J_0+1)}\left[\sum_{\kappa,\kappa'}(-1)^{J_0+L+J_i-1/2}(-1)^{(l-l')/2}\cos(\delta_\kappa-\delta_{\kappa'})\right.$$
$$\left.\times[j,j',l,l',L]^{1/2}\begin{pmatrix}l & l' & L\\ 0 & 0 & 0\end{pmatrix}\begin{Bmatrix}j' & j & L\\ l & l' & \frac{1}{2}\end{Bmatrix}\begin{Bmatrix}J_i & J_i & L\\ j & j' & J_0\end{Bmatrix}\langle J_i\|V\|J_0jJ_i\rangle\langle J_i\|V\|J_0j'J_i\rangle^*\right] . \tag{6}$$

Here l, j, and $\kappa=(l-j)(2j+1)$ are the quantum numbers for the partial wave; J_0, J_i, and J_f are the total angular momenta for the initial ionic state, intermediate autoionizing, and stabilized x-ray final states of the projectile, respectively; δ_κ is the phase shift; $\langle J_i\|V\|J_0jJ_i\rangle$ is the reduced Auger matrix element; $P_2(\cos\theta)=\frac{1}{2}(3\cos^2\theta-1)$; $[a,b,c,\ldots]^{1/2}=[(2a+1)(2b+1)(2c+1)\cdots]^{1/2}$; and θ is the angle of emission of x-ray with respect to the beam axis in the projectile frame.

For the chlorinelike ions in collisions with H_2 targets, the RTEX process through *LMM* inverse Auger transitions

TABLE I. Resonance energies and resonance strengths for the 15 strongest *LMM* dielectronic recombination resonances in Fe^{9+}.

Initial state	Autoionizing state	Energy (eV)	Strength (10^{-20} cm^2 eV)
$^2P_{3/2}$	$[(2p^*)_{1/2}3d^*]_1$	523.0	0.763
	$[(2p3p)_3(3d^2)_4]_5$	562.9	0.354
	$\{[(2p^*3p)_1 3d^*]_{5/2}3d\}_4$	565.9	0.386
	$[(2p3p^*)_2(3d^2)_4]_4$	566.7	0.602
	$[(2p^*3p)_2(3d^{*2})_2]_3$	571.8	0.983
	$[(2p^*3p)_1(3d^{*2})_2]_2$	571.9	0.510
	$[(2p^*3p)_2(3d^{*2})_2]_4$	572.9	0.435
	$[(2p^*3p)_1(3d^2)_2]_3$	574.8	0.593
	$\{[(2p^*3p)_1 3d^*]_{5/2}3d\}_5$	577.5	0.424
	$[(2p^*3p)_1(3d^{*2})_2]_3$	578.9	0.740
	$\{[(2p^*3p)_2 3d^*]_{3/2}3d\}_3$	581.6	0.393
	$\{[(2p^*3p)_2 3d^*]_{5/2}3d\}_2$	592.1	0.313
	$\{[(2s3p)_2 3d^*]_{7/2}3d\}_6$	700.9	0.345
	$\{[(2s3p)_2 3d^*]_{5/2}3d\}_5$	701.5	0.255
	$\{[(2s3p)_1 3d^*]_{5/2}3d\}_5$	703.7	0.353
$^2P_{1/2}$	$[(2p)_{3/2}3d]_1$	509.3	0.430
	$[(2p^*)_{1/2}3d]_1$	521.1	0.355
	$\{[(2p3p^*)_1 3d^*]_{1/2}3d\}_3$	561.5	0.353
	$\{[(2p^*3p^*)_1 3d^*]_{5/2}3d\}_3$	568.0	0.957
	$[(2p^*3p^*)_1(3d^{*2})_2]_3$	568.3	1.20
	$[(2p^*3p^*)_1(3d^{*2})_2]_2$	572.5	0.812
	$[(2p^*3p)_1(3d^2)_2]_3$	572.9	0.457
	$\{[(2p^*3p)_2 3d^*]_{3/2}3d\}_4$	574.5	0.825
	$[(2p^*3p)_1(3d^{*2})_2]_3$	574.9	0.418
	$[(2p^*3p)_2(3d^{*2})_2]_2$	575.0	0.338
	$\{[(2p^*3p^*)_1 3d^*]_{3/2}3d\}_4$	577.5	1.36
	$\{[(2p^*3p)_2 3d^*]_{5/2}3d\}_3$	578.7	1.23
	$\{[(2p^*3p)_2 3d^*]_{3/2}3d\}_3$	579.7	0.427
	$\{[(2p^*3p^*)_1 3d^*]_{1/2}3d\}_3$	587.3	0.329
	$\{[(2s3p)_1 3d^*]_{3/2}3d\}_5$	701.7	0.439

can be schematically represented by

$$A^{q+}(1s^22s^22p^63s^23p^5)+H_2 \rightarrow A^{(q-1)+}(1s^22s^22p^53s^23p^m3d^t)+H_2^+$$
$$\hookrightarrow A^{(q-1)+}(1s^22s^22p^63s3p^m3d^t)+h\nu$$
$$\hookrightarrow A^{(q-1)+}(1s^22s^22p^63s^23p^m3d^{t-1})+h\nu' , \quad (7)$$

and

$$A^{q+}(1s^22s^22p^63s^23p^5)+H_2 \rightarrow A^{(q-1)+}(1s^22s2p^63p^m3d^t)+H_2^+$$
$$\hookrightarrow A^{(q-1)+}(1s^22s^22p^63s^23p^{m-1}3d^t)+h\nu . \quad (8)$$

In Eqs. (7) and (8), the possible intermediate configurations for the *LMM* transitions are $m=6$, $t=1$ and $m=5$, $t=2$.

The Auger transitions via Coulomb interaction and radiative electron-dipole transition rates for each autoionizing state were calculated using the first-order perturbation theory and the MCDF model [17,18]. The atomic energy levels and bound-state wave functions were evaluated in intermediate coupling with configuration interaction using the MCDF model in an extended-averaged level scheme [18]. In the calculations of autoionizing states, we included 362 states from the $1s^22s2p^63s^23p^63d$, $1s^22s2p^63s^23p^53d^2$, $1s^22s^22p^53s^23p^63d$, and $1s^22s^22p^53s^23p^53d^2$ configurations. For the Auger final states, 453 states from the $3p^63d$, $3s3p^53d$, $3s3p^6$, $3s^23p^43d$, $3s^23p^5$, $3p^53d^2$, $3s3p^43d^2$, and $3s^23p^33d^2$ configurations were taken into account. Here, the Ne core $1s^22s^22p^6$ is omitted in the above descriptions. The x-ray final states consist of 218 states arising from $3s^23p^6$, $3s3p^63d$, $3s3p^53d^2$, $3s^23p^53d$, and $3s^23p^43d^2$

TABLE II. Resonance energies and resonance strengths for the 15 strongest *LMM* dielectronic recombination resonances in Nb^{24+}.

Initial state	Autoionizing state	Energy (eV)	Strength (10^{-20} cm^2 eV)
$^2P_{3/2}$	$[(2p)_{3/2}3d]_1$	1138.7	2.45
	$[(2p^*)_{1/2}3d^*]_1$	1224.6	3.70
	$\{[(2p3p)_2 3d^*]_{5/2}3d\}_1$	1241.9	3.09
	$[(2p3p)_3(3d^2)_4]_2$	1243.4	2.51
	$\{[(2p3p)_3 3d^*]_{5/2}3d\}_3$	1244.4	2.00
	$[(2p3p)_3(3d^2)_4]_5$	1246.0	2.56
	$\{[(2p3p)_2 3d^*]_{7/2}3d]_4$	1251.6	5.99
	$[(2p3p)_2(3d^2)_2]_4$	1251.7	3.49
	$\{[(2p3p)_2 3d^*]_{3/2}3d\}_3$	1254.9	6.94
	$\{[(2p3p^*)_2 3d^*]_{5/2}3d\}_2$	1260.1	2.04
	$\{[(2p^*3p)_1 3d^*]_{5/2}3d\}_5$	1340.3	2.85
	$\{[(2p^*3p)_2 3d^*]_{5/2}3d\}_5$	1342.8	2.84
	$\{[(2p^*3p)_2 3d^*]_{3/2}3d\}_4$	1350.0	6.09
	$\{[(2s3p)_2 3d^*]_{7/2}3d\}_6$	1576.6	2.32
	$\{[(2s3p)_1 3d^*]_{5/2}3d\}_5$	1575.0	2.66
$^2P_{1/2}$	$[(2p)_{3/2}3d]_1$	1118.1	6.42
	$\{[(2p3p^*)_2 3d^*]_{5/2}3d\}_2$	1249.0	3.90
	$[(2p3p^*)_1(3d^2)_4]_3$	1250.1	8.49
	$[(2p3p^*)_2(3d^2)_4]_3$	1251.8	15.8
	$[(2p3p^*)_2(3d^2)_2]_2$	1254.2	4.78
	$[(2p3p^*)_2(3d^2)_4]_4$	1254.8	6.31
	$\{[(2p3p^*)_2 3d^*]_{1/2}3d\}_3$	1259.6	3.93
	$[(2p3p^*)_2(3d^{*2})_0]_2$	1265.9	1.97
	$\{[(2p3p^*)_2 3d^*]_{3/2}3d\}_2$	1277.6	7.99
	$\{[(2p^*3p^*)_0 3d^*]_{3/2}3d\}_3$	1341.5	6.19
	$\{[(2p^*3p^*)_1 3d^*]_{3/2}3d\}_4$	1342.3	7.52
	$\{[(2p^*3p^*)_1 3d^*]_{1/2}3d\}_3$	1354.2	8.71
	$\{[(2s3p^*)_1 3d^*]_{5/2}3d\}_4$	1571.1	2.24
	$\{[(2s3p^*)_1 3d^*]_{5/2}3d\}_5$	1573.4	4.43
	$\{[(2s3p^*)_1 3d^*]_{3/2}3d\}_4$	1586.8	2.33

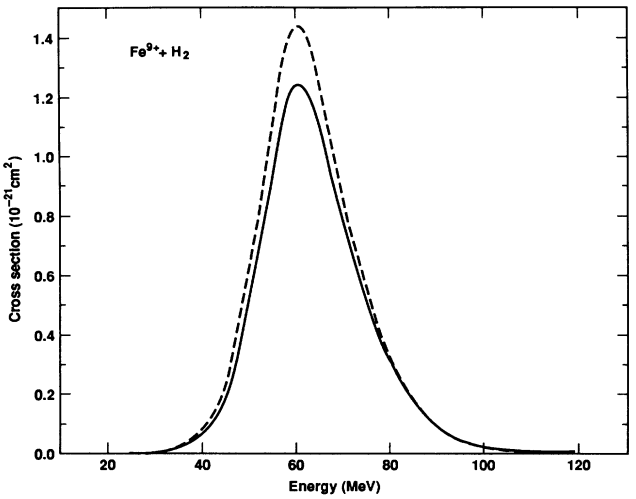

FIG. 1. The *LMM* RTEX cross sections in collisions of Fe^{9+} with H_2 from this work as functions of projectile energy. The dashed curve indicates the results for the $^2P_{1/2}$ state, and the solid curve represents the values for the $^2P_{3/2}$ state.

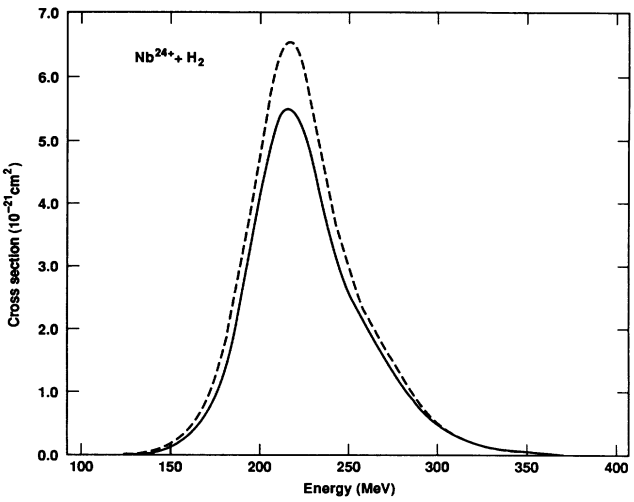

FIG. 2. The *LMM* RTEX cross sections in collisions of Nb^{24+} with H_2. The symbols are the same as in Fig. 1.

TABLE III. Resonance energies and resonance strengths for the 15 strongest *LMM* dielectronic recombination resonances in La^{40+}.

Initial state	Autoionizing state	Energy (eV)	Strength (10^{-20} cm^2 eV)
$^2P_{3/2}$	$[(2p)_{3/2}3d]_1$	1993.1	7.13
	$[(2p3p)_3(3d^2)_2]_5$	2156.2	10.4
	$\{[(2p3p)_3 3d^*]_{7/2}3d\}_4$	2161.4	32.9
	$\{[(2p3p)_2 3d^*]_{7/2}3d\}_3$	2171.0	21.0
	$[(2p3p)_3(3d^2)_4]_5$	2174.8	14.1
	$[(2p3p)_1(3d^2)_4]_3$	2175.4	12.3
	$\{[(2p3p)_3 3d^*]_{9/2}3d\}_2$	2177.2	9.61
	$\{[(2p3p)_0 3d^*]_{3/2}3d\}_4$	2179.4	10.2
	$\{[(2p3p)_2 3d^*]_{3/2}3d\}_3$	2180.4	6.14
	$[(2p3p)_3(3d^2)_4]_4$	2183.6	22.1
	$[(2p3p)_3(3d^2)_4]_3$	2198.1	6.93
	$[(2p3p)_2(3d^2)_4]_2$	2215.8	6.88
	$\{[(2p^*3p)_2 3d^*]_{5/2}3d\}_3$	2574.2	6.89
	$[(2p^*3p)_1(3d^2)_4]_5$	2578.4	9.00
	$\{[(2p^*3p)_2 3d^*]_{5/2}3d\}_4$	2589.3	8.71
$^2P_{1/2}$	$[(2p)_{3/2}3d]_1$	1893.0	15.5
	$[(2p3p^*)_2(3d^2)_2]_3$	2167.0	7.23
	$\{[(2p3p^*)_1 3d^*]_{5/2}3d\}_3$	2170.2	52.1
	$[(2p3p^*)_2(3d^2)_4]_3$	2186.3	22.1
	$[(2p3p^*)_2(3d^2)_4]_4$	2189.1	29.7
	$[(2p3p^*)_2(3d^2)_4]_2$	2190.3	27.6
	$\{[(2p3p^*)_2 3d^*]_{3/2}3d\}_2$	2201.0	24.9
	$[(2p3p^*)_2(3d^2)_0]_2$	2202.7	10.2
	$[(2p^*3p^*)_1(3d^{*2})_2]_3$	2527.7	6.01
	$\{[(2p^*3p^*)_1 3d^*]_{3/2}\}_3$	2572.2	10.4
	$\{[(2p^*3p^*)_1 3d^*]_{3/2}3d\}_4$	2576.4	34.4
	$\{[(2p^*3p^*)_1 3d^*]_{1/2}3d\}_3$	2587.1	28.1
	$\{[(2s3p^*)_0 3d^*]_{3/2}3d\}_4$	2930.7	6.40
	$[(2s3p^*)_1(3d^2)_4]_5$	2944.8	6.76
	$\{[(2s3p^*)_1 3d^*]_{3/2}3d\}_4$	2950.3	6.08

configurations. The effects of the Breit interaction and quantum-electrodynamic corrections were included in the calculations of transition energies.

The RTEX cross sections were computed according to Eqs. (1)–(6) with the energy-averaged DR cross sections calculated using Eq. (3). The angular distribution function $W(\theta)$ was evaluated using Eqs. (4)–(6). The phase shifts in Eq. (6) were calculated according to a procedure outlined by Zhang, Sampson, and Clark [22]. The Compton profile for H_2 was taken from experiment [23].

In order to study the effect of relativity on the RTEX cross sections, the nonrelativistic energies and transition rates were obtained by repeating the MCDF calculations for La^{40+} with the velocity of light increased a thousandfold [18].

III. RESULTS AND DISCUSSION

The resonance energies and resonance strengths from Eq. (3) for the 15 strongest *LMM* DR resonances in Fe^{9+}, Nb^{24+}, and La^{40+} are listed in Tables I, II, and III, respectively. The atomic states are identified by the dominant *jj* component in the basis set expansion. The symbols nl^* and nl (e.g., $2p^*$ and $2p$) indicate the subshells with $j=l-\frac{1}{2}$ and $j=l+\frac{1}{2}$, respectively. The notation $\{[(2p^*3p)_1 3d^*]_{5/2}3d\}_4$ represents a state formed by coupling a hole in a $2p_{1/2}$ shell and a hole in a $3p_{3/2}$ shell to yield an intermediate quantum number $J=1$ then coupled with an electron in a $3d_{3/2}$ shell to give $J=5/2$ and finally coupled with an electron in a $3d_{5/2}$ shell to make a total angular momentum $J=4$. In this description, the full shells in the electronic configurations are omitted. The sum of the resonance strengths for the top 15 DR resonances is about 50% of the total LMM resonance strength.

The RTEX cross sections without corrections for the angular distribution for Fe^{9+} and Nb^{24+} in collisions with H_2 are displayed in Figs. 1 and 2, respectively. The cross sections for the $^2P_{1/2}$ state are seen to be larger than those for the $^2P_{3/2}$ state at the peak by 15% for Fe^{9+} and by 20% for Nb^{24+} due to the effects of relativity and spin-orbit coupling.

In Fig. 3, the RTEX cross sections for La^{40+} in collisions with H_2 from the nonrelativistic and relativistic calculations are compared. The relativistic results show three-hump structure, while the nonrelativistic calculations yield a single peak. The peak height for the nonrelativistic theory is about twice as large as the peak height for the relativistic case. The total nonrelativistic DR strength is larger than the relativistic one by 29%. The cross sections for the $^2P_{1/2}$ state from the MCDF calculations show a much stronger second peak at 6.5 MeV as compared to the second peak for the $^2P_{3/2}$ state.

The RTEX cross sections for the La^{40+} ions in collisions with H_2 from the MCDF model including the angular distribution corrections at $\theta=90°$ are compared with experiment [19] in Fig. 4. The effect of angular distribution at $\theta=90°$ increases the cross sections by an amount less than 10%. One can see that the experimental results agree much better with the cross sections for

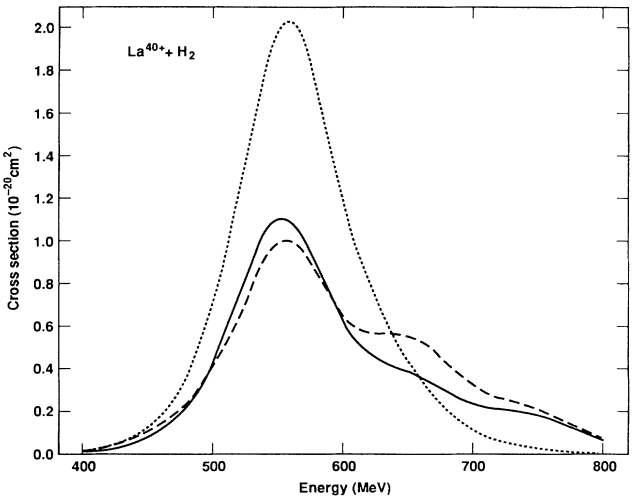

FIG. 3. The *LMM* RTEX cross sections in collisions of La^{40+} with H_2. The solid curve displays the results for the $^2P_{3/2}$ state and the dashed curve indicates the values for the $^2P_{1/2}$ state using the relativistic Hartree-Fock method. The dotted curve illustrates the predictions from the nonrelativistic *LS* coupling calculations.

the $^2P_{1/2}$ excited state than with those for the $^2P_{3/2}$ ground state. At low energies, the theory slightly underestimates the cross sections.

In summary, we have calculated the RTEX cross sections from *LMM* transitions for the chlorinelike Fe^{9+}, Nb^{24+}, and La^{40+} in collisions with H_2 using the impulse approximation and the MCDF method. The cross sections for the $^2P_{1/2}$ state can differ by as much as 20% from the cross sections for the $^2P_{3/2}$ state. For the La^{40+}

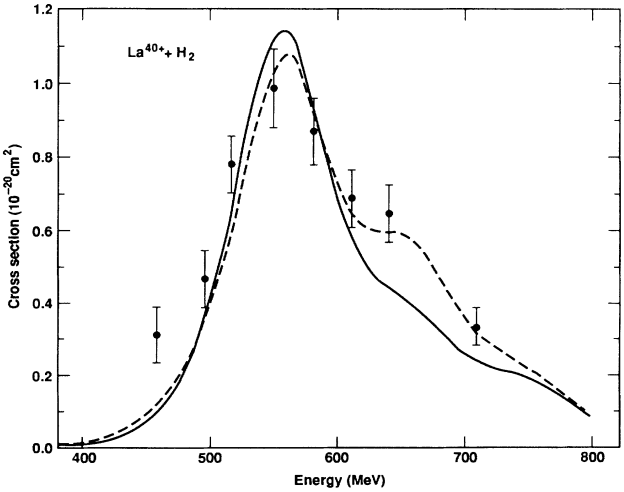

FIG. 4. The experimental and theoretical RTEX cross sections in collisions of La^{40+} with H_2 are compared. The symbols are the same as in Fig. 1. The experimental data are taken from Ref. [19].

ion, the effect of relativity reduces the cross sections by 29%. The effect of the angular distribution at $\theta=90°$ increases the cross sections by $\leq 10\%$. The theoretical predictions from the MCDF calculations are in reasonable agreement with the experimental findings for La^{40+}.

ACKNOWLEDGMENT

This work was performed under the auspices of the U.S. Department of Energy by Lawrence Livermore National Laboratory under Contract No. W-7405-Eng-48.

[1] D. Brandt, Phys. Rev. A **27**, 1314 (1983).
[2] J. A. Tanis, S. M. Shafroth, J. E. Willis, M. Clark, J. Swenson, E. N. Strait, and J. R. Mowat, Phys. Rev. Lett. **47**, 828 (1981).
[3] Y. Hahn, Phys. Rev. A **40**, 2950 (1989).
[4] J. A. Tanis, E. M. Bernstein, W. G. Graham, M. Clark, S. M. Shafroth, B. M. Johnson, K. W. Jones, and M. Meron, Phys. Rev. Lett. **49**, 1325 (1982).
[5] J. A. Tanis, E. M. Bernstein, M. P. Stockli, M. Clark, R. H. McFarland, T. J. Morgan, K. H. Berkner, A. Schlacter, and J. W. Stearns, Phys. Rev. Lett. **53**, 2551 (1984).
[6] J. A. Tanis, E. M. Bernstein, M. W. Clark, W. G. Graham, R. H. McFarland, T. J. Morgan, J. R. Mowat, D. W. Mueller, A. Müller, M. P. Stockli, K. H. Berkner, P. Gohil, R. J. McDonald, A. S. Schlacter, and J. W. Stearns, Phys. Rev. A **34**, 2543 (1986).
[7] M. Schultz, R. Schuch, S. Datz, E. L. B. Justiniano, P. D. Miller, and H. Schöne, Phys. Rev. A **38**, 5454 (1988).
[8] W. G. Graham, K. H. Berkner, E. M. Bernstein, M. W. Clark, B. Feinberg, M. A. McMaham, T. J. Morgan, W. Rathbun, A. S. Schlachter, and J. A. Tanis, Phys. Rev. Lett. **65**, 2773 (1990).
[9] J. M. Feagin, J. S. Briggs, and T. M. Reeves, J. Phys. B **17**, 1057 (1984).
[10] D. J. McLaughlin and Y. Hahn, Phys. Lett. **112A**, 389 (1985); Phys. Rev. A **37**, 3587 (1988).
[11] N. R. Badnell, Phys. Rev. A **40**, 3579 (1989).
[12] C. P. Bhalla and K. R. Karim, Phys. Rev. A **39**, 6060 (1989).
[13] M. H. Chen, Phys. Rev. A **41**, 4102 (1990); Nucl. Instrum. Methods **B56/57**, 149 (1991); Phys. Rev. A **42**, 5228 (1990).
[14] N. R. Badnell, Phys. Rev. A **42**, 204 (1990).
[15] M. S. Pindzola and N. R. Badnell, Phys. Rev. A **42**, 6526 (1990).
[16] E. M. Bernstein *et al.*, Abstracts of contributed papers, in *The Sixteenth International Conference on The Physics of Electronic and Atomic Collisions, 1989,* edited by A. Dalgarno, R. S. Freund, M. S. Lubell, and T. B. Lucatorto (unpublished), p. 553.
[17] M. H. Chen, Phys. Rev. A **31**, 1449 (1985).
[18] I. P. Grant, B. J. McKenzie, P. H. Norrington, D. F. Mayers, and N. C. Pyper, Comput. Phys. Commun. **21**, 207 (1980).
[19] E. M. Bernstein *et al.*, J. Phys. B **20**, L505 (1987).
[20] A. Itoh, T. J. M. Zouros, D. Schneider, U. Stettner, W. Zeitz, and N. Stolterfoht, J. Phys. B **18**, 4581 (1985).
[21] C. P. Bhalla, Phys. Rev. Lett. **64**, 1103 (1990).
[22] H. L. Zhang, D. H. Sampson, and R. E. H. Clark, Phys. Rev. A **41**, 198 (1990).
[23] J. S. Lee, Chem. Phys. **66**, 4906 (1977).